Applied Ocean Research 113 (2021) 102721

Contents lists available at ScienceDirect

Applied Ocean Research

journal homepage: www.elsevier.com/locate/apor

The variability of marine sediment erodibility with depth: Centimetric scale effects detected from portable erosion flume tests

Henning Mohr [*,a], Samuel A. Stanier [b], David J. White [c], Matthew Kuo [d]

[a] Wave Energy Research Centre, The University of Western Australia, 35 Stirling Highway, Crawley, WA 6009, Australia
[b] University of Cambridge, Department of Engineering, 7a JJ Thompson Avenue, Cambridge CB3 0FA, UK
[c] University of Southampton, Boldrewood Innovation Campus, Southampton SO16 7QF, United Kingdom
[d] The University of Western Australia, 35 Stirling Highway, Crawley, WA 6009, Australia

ARTICLE INFO

Keywords:
Portable erosion flume
Erosion threshold
Erosion rate
Marine sediments
Scour prediction
Subsea pipelines

ABSTRACT

A portable erosion flume has been developed that is capable of estimating erosion threshold and erosion rate relationships for fine-grained specimens over the depth of a typical sample tube. This newly-designed apparatus is a recirculating flume capable of generating steady currents over the exposed section of the sample. In this paper, the erosion properties of two marine sediments have been determined and show a significant systematic variation with depth at centimetre scale that would have implications for the potential need for scour protection engineering. The tests showed that the critical erosion onset velocity doubled over the upper 200 mm of each sample, and the erosion rate fell by an order of magnitude. The increased erosion resistance with depth is consistent with the general trend of erodibility reducing with decreasing moisture content. Ignoring this depth effect when selecting design values of the erosion properties could lead to erroneous predictions of scour rate and extent around subsea structures, and unnecessary scour protection engineering costs.

1. Introduction

The placement of offshore structures such as subsea cables, pipelines, or foundations on the seabed may result in the removal of sediment due to the amplification of the fluid flow around the structure (i.e. scour). Depending on the magnitude and rate of scour, the stability and integrity of the subsea structure may be compromised, or potentially enhanced (Leckie et al., 2015). To predict scour, the flow conditions and the erosion properties must be determined, and scour is also affected by the shape and size of the structure (e.g. Draper et al., 2017 or Whitehouse, 1998).

Seabed erosion properties are well known for uniform sands and predictive formulas for the ultimate depth and rate of scour in sands are widely used in engineering practice. The mechanisms of scour around hydraulic structures have been summarised in detail by Sumer et al. (2002) with the most prominent examples being scour around bridge piers or underneath pipelines. A comprehensive overview of models for sand predicting the temporal scour depth variation and equilibrium scour depths around bridge piers can be found in Pandey et al. (2017). For pipelines in sand, empirical formulas have been developed to predict the scour development and can be found in Fredsøe et al. (1992), Kjeldsen et al. (1973) or Mao (1986).

In practice, however, real marine sediments of a silty nature can have very different erosion properties compared to clean sands, leading to delayed scour development: see for example Kjeldsen et al. (1973), Briaud et al. (1999), Rambabu et al. (2003), Mohr et al. (2016) or Tom et al. (2016). For example, Roberts et al. (1998) and Mitchener and Torfs (1996) show that the erosion rates for fine-grained sediments depend heavily on the bulk sediment properties, which may vary spatially. Approaches to assess scour often do not consider the variability of the erosion properties over the potential scour depth, but this variation may actually be beneficial to the overall stability of the subsea structure.

Previous research measured this depth variability of the erosion properties with straight flumes that allowed the insertion of a sediment core sample into the flume at the open bottom of the test section. The following flumes accommodate this type of testing: the (i) SEDflume (Jepsen et al., 1997; McNeil et al., 1996; Roberts et al., 1998); the ASSET flume (Roberts et al., 2003); the Erosion Function Apparatus (EFA) (Briaud et al., 1999); the SETEG flume (Kern et al., 1999; Noack et al., 2015) and the Erodimetre (Jacobs et al., 2011). These laboratory flumes allow for a relatively controlled measurement of the erosion properties with sample depth, however, ex-situ samples may be disturbed during

* Corresponding author.
E-mail addresses: henning.mohr@uwa.edu.au (H. Mohr), sas229@cam.ac.uk (S.A. Stanier), david.white@soton.ac.uk (D.J. White).

https://doi.org/10.1016/j.apor.2021.102721
Received 1 September 2020; Received in revised form 6 May 2021; Accepted 15 May 2021
Available online 21 June 2021

Nomenclature

η	Erosion rate
η_{avg}	Depth-averaged erosion rate
ν	Viscosity
ρ_w	Density of water
τ	Bed shear stress
τ_{amp}	Amplified bed shear stress
U_{cr}	Threshold velocity at an erosion rate of 3e-7 m/s
τ_{free}	Free field bed shear stress
θ_{cr}	Dimensionless threshold shear stress at an erosion rate of 3e-7 m/s
d_{50}	Median grain size
G_s	Specific gravity
M	Fitting parameter for Eq. (4) and n
n	Fitting parameter for Eq. (4)
S	Scour depth
S_e	Equilibrium scour depth
t	Time
T_{avg}	Depth-averaged time scale
$U(z)$	Measured velocity 20 mm above the bed
u^*	Friction velocity
τ_{cr}	Threshold shear stress at an erosion rate of 3e-7 m/s
w	Water content
z	Depth
Clay	Clay content
Fines	Fines content

storage and transportation prior to testing leading to alterations in their mechanical, biological or chemical properties. Furthermore, this type of erosion testing of samples is time-consuming in that samples must be recovered from the seabed, transported for testing, prepared for testing and then tested before results are obtained.

In contrast, in-situ erosion testing reduces the potential for sample

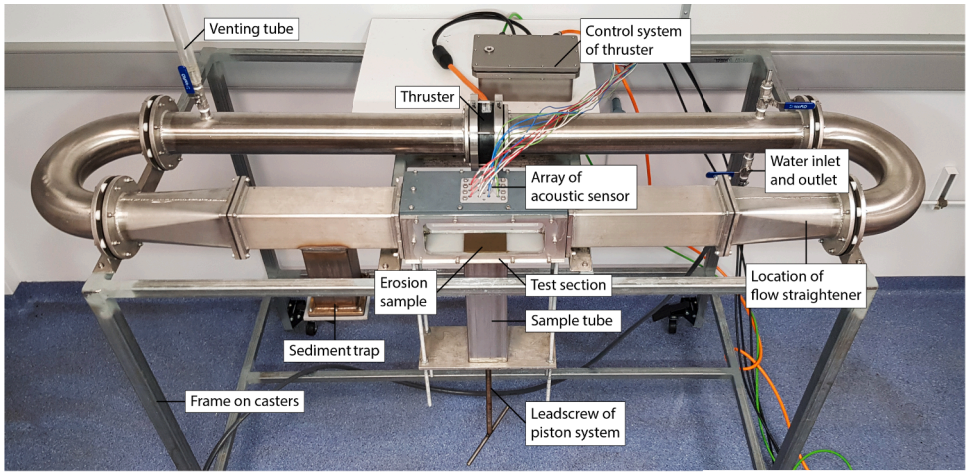

(a) Layout of portable erosion flume.

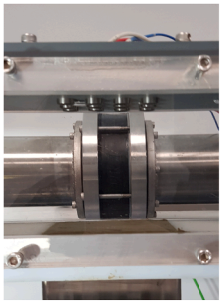

(b) Test-section.

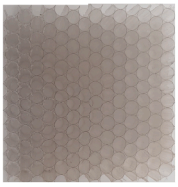

(c) Flow straightener.

(d) Rim-driven thruster.

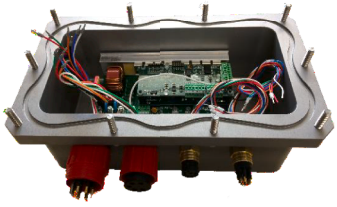

(e) Control system.

Fig. 1. Photographs of portable erosion flume and components.

disturbance. However, current methods generally lack the capability to obtain an erosion profile with depth and are cumbersome and time consuming to deploy, which might result in significant extension of the duration of a survey unless other activities can be conducted in parallel. Examples include: the SEADUCT (Nowell and Hollister, 1985); the Circular sea carousel (Amos et al., 1992); the VIMS sea carousel (Maa et al., 1993); the SEAFLUME (Gust and Morris, 1989; Young, 1977); the Portable straight flume (Ravens and Gschwend, 1999); or NIWA I/II (Debnath et al., 2007).

The paper presents a portable erosion apparatus that allows effective field testing (i.e. on-board of a vessel or at an onshore site) due to its compact and rugged design. To demonstrate its capabilities, two core samples of fine-grained soil sediment from offshore have been investigated regarding their depth variability of the erosion properties by testing multiple layers within a "Shelby" tube. The erosion measurements are then related to a typical scour assessment of a subsea structure (i.e. pipeline) with a subsequent discussion on the design significance of depth-varying erosion properties. The advantages of the apparatus are three-fold:

1. Tests can be performed during the survey with real-time feedback to the design engineer allowing survey scope to be adjusted where beneficial;
2. Samples can be collected and tested with minimal risk of extension of the survey duration (the samples are tested "off the critical path" of the survey operations); and
3. Samples do not need to be transported back to an onshore laboratory, which minimises the risk of damage during transit and storage.

2. Experimental setup

A portable erosion flume was developed for estimating the erosion threshold and erosion rate relationships of fine-grained and coarse-grained sediments using small tube samples. This newly designed apparatus is a recirculating flume capable of generating steady currents over the erosion sample (see Fig. 1). It represents an evolution of previous flumes that have been used to study erosion behaviour in-situ and in the laboratory, but which have not yet evolved into tools used routinely in geotechnical site investigation practice (e.g. Young (1977), Amos et al. (1992), Ravens and Gschwend (1999), Debnath et al. (2007)).

The portable erosion apparatus is 2 m long and 0.5 m wide with a square test section with a cross section of 94 mm by 94 mm and transparent plastic viewing windows. As shown in Fig. 1 (a), it is mounted on a 1.5 m high frame allowing the attachment of a 500 mm long soil sample tube below the test section. Using a piston mechanism, the sediment within the sample tube can be pushed into the test section in controlled steps via an opening in the test section base. This allows successive testing of the erosion properties of several layers throughout the depth of the tube sample.

To produce a steady current, a rim-driven thruster made by Enitech is embedded in the duct of the flume opposite to the test section. As shown in Fig. 1 (c), the thruster has its blades mounted on a cylindrical ring which is also the rotor of the electric motor. The hubless design offers the advantage of reduced secondary flows (Lee and Chen, 2007; Yakovlev et al., 2011). To further reduce secondary flows, a flow straightener is mounted upstream of the eroding sample with straightening tubes of 6 mm (see Fig. 1 (d)).

To measure the total load transport (i.e. both bedload and suspended load transport), a total of 12 acoustic distance sensors are mounted above the erosion sample providing a continuous measurement of the averaged eroding volume over time (see Fig. 1 (b)). The 5 MHz acoustic transducer sends and receives acoustic signals and calculates the distance between sensor and reflected object based on the speed of sound in water. The measuring distance of the transducer ranges between 30 mm to 1100 mm exhibiting an accuracy of +/- 0.1 mm and sampling rates of up to 50 Hz. The system is insensitive to small amounts of suspended sediment in the flow compared to conventional measurement methods (e.g. laser scanner). Any erroneous data points due to obstructions in the flow can be filtered because of the high sample frequency and/or the use of blanking distances.

3. Experimental procedure

3.1. Calibration and shear stress determination

Prior to conducting erosion testing, the flow velocity profile produced by the thruster was measured for different rotational speeds above a smooth bed over the sample location. The streamwise velocity measurements were performed over a region close to the flume bed using a Nortek Vectrino-II Acoustic Doppler Velocimeter (ADV) Profiler. During erosion testing, the rotational speed of the thruster was measured continuously and linked to the velocity measurements based on these calibration tests. Fig. 2 shows data obtained from this initial calibration using a velocity reading at a height of 20 mm above the bed. For the applied range of shear stress, the Reynolds numbers, UD/ν, are on the order 10^5 to 10^6 suggesting a turbulent flow, except for very low discharges. The mean velocities measured with the ADV are transformed to shear stresses by assuming a logarithmic velocity distribution (which seemed reasonable based on the velocity profile measurements and has been used in similar studies; e.g. Ye et al. (2011), Mohr et al. (2020)) close to the test bed and the empirical expression of the seabed roughness length (z_0).

To convert velocity to shear stress, the velocity measured by the ADV for each rotational speed setting has been converted into friction velocity, u^*, by solving the following equation numerically:

$$U(z) = \frac{u^*}{0.4}\ln\left(\frac{z}{z_0}\right), \tag{1}$$

where $U(z)$ is the measured velocity above the bed (e.g. $z = 20$ mm), ν is the viscosity of water (assumed to be 1.003 x 10^{-6} m^2/s).

The bed roughness length z_0 in Equation (1) for a hydrodynamically smooth flow as suggested by Colebrook and White (1937) can be expressed as:

$$z_0 = \frac{\nu}{9u^*}, \tag{2}$$

A hydrodynamically smooth flow is given when $u^*k_s/\nu < 5$ which is the case for both measured median grain sizes using the expression from Sleath (1984) with $k_s = 2.5d_{50}$. As Equation (2) is independent of the roughness, it was not deemed necessary to match the pipe roughness

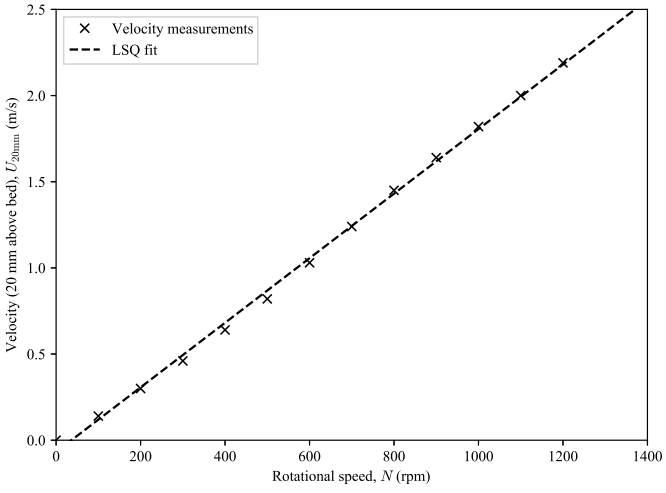

Fig. 2. Calibration of flow pump.

with the sample roughness.

The bed shear stress τ is then given in terms of the friction velocity according to:

$$\tau = \rho_w u^{*2} , \quad (3)$$

where ρ_w is the density of water (taken as 998 kg/m^3). Equations (1) – (3) assume that the velocity profile near the bed is logarithmic, and that the velocity measured at 20 mm above the bed changes minimally for a given rotational speed setting with the introduction of a soil sample.

In summary, the calibration of the bed shear stress presented enables the discussion of relative variations of the erosion properties and is only applicable to the flow range and samples tested ($d_{50} < 0.02$ mm) within this study. Care should be taken when discussing absolute shear stress values when comparing results with other studies that used different apparatus or samples.

3.2. Test procedure

A square sample tube was installed below the test section and pushed using a piston mechanism until the desired depth within the sample for erosion testing was level with the base of the channel. Conventional circular sample tubes can also be used in the system, however, the square sample tubes are preferred because they maximise the sample surface area over which the scour properties are measured, and simplify the interpretation of the average erosion rate somewhat. Excess material was carefully removed and the final testing surface gently levelled prior to the start of each test.

Erosion testing was performed under steady flow conditions. In each test, a steady current velocity (at 20 mm above bed) was introduced starting at ~0.15 m/s for sandy sediments. The water velocity was then increased in ~0.15 m/s increments up to ~2.15 m/s in initially 10 minutes intervals until threshold was reached and reduced depending on the progress of erosion. During each velocity step, the erosion depth was continuously measured at 10 Hz using the array of acoustic sensors system above the sample surface. This allowed for the calculation of the average erosion rate over the sample surface by fitting a linear expression with respect to the depth measurement over time. To avoid edge effects, the averaging was done over a square area which excluded the outer 10% of the sample closest to the boundary (see Fig. 3). A linear continuous measurement of the erosion progress also indicated that changes in shear stress with the measured erosion depth were minimal. Furthermore, throughout the testing process, the bed level was always kept flush within 1.5 mm of the flume bed in order to avoid any potential effect of reducing shear stress with increasing erosion depth. This required the reduction of the erosion time interval for highly erodible flow velocities. The erosion rate is defined as the average change in height of the sample (in m) over this area, divided by the time period of testing (in s).

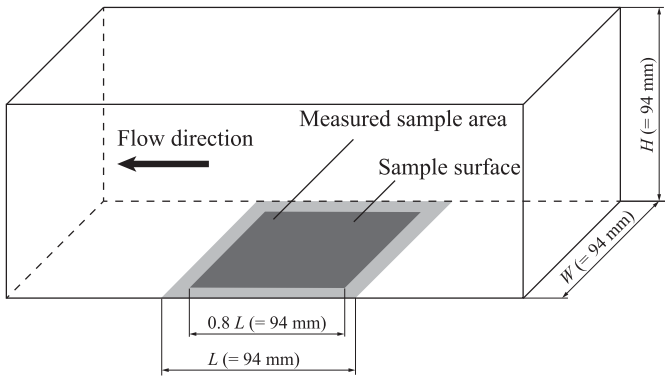

Fig. 3. Schematic view of soil sample in working section. L is the length and width of the square sample surface.

The threshold shear stress is defined as the bed shear stress corresponding to significant erosion, which equates to an erosion rate of approximately 3e-7 m/s, or 1 mm/hour. This definition of threshold shear stress leads to an estimate that is solely determined by the measurements and is less subjective than some other definitions (e.g. Briaud et al., 1999; Buffington and Montgomery, 1997; Mohr, 2015; Roberts et al., 1998). To accurately and objectively identify a specific erosion rate as low as 3e-7 m/s, the erosion rate measurements have been least squares fitted using the following expression:

$$\eta = M\tau^n , \quad (4)$$

where η is the erosion rate, τ is the shear stress, and M and n are fitting parameters. This expression is then used to extrapolate or interpolate to 3e-7 m/s. Equation (4) is a commonly used fit for erosion measurements; see for example Roberts et al. (1998).

4. Erosion testing

Two soil samples, referred to as S1 and S2, were recovered from box cores taken at a location offshore and tested to identify their erosion properties at multiple depths within each sample. The samples were obtained in the same project soil zone and were both given the visual description of olive slightly sandy CLAY when sub-sampled from the box cores.

Each of the samples was extruded smoothly into the test section and trimmed flush to the bed of the flume. The colour and the grain size of the samples appeared uniform across each tested depth. Sample S1 appeared to be composed of slightly coarser material than sample S2, in particular in the upper layers of the sample (see particle size distribution in Fig. 4). See Table 1 for the geotechnical properties of the two samples, each extracted from the same boxcore sample, that were used to interpret the erosion tests (d_{50} and G_s).

Fig. 5 shows the erosion rate measurements for both soil samples for 5 different depth layers (50 mm, 100 mm, 150 mm, 200 mm and 250 mm), which results in a total of 10 individual erosion tests (see also the testing summary given in Table 2). The data are fitted using a least squares method to Equation (4). The derived threshold shear stress is determined by the point of intersection between the least squares fit and the threshold erosion rate of 3e-7 m/s (indicated as a dashed line). The erosion rate decreases with depth (and reducing water content) in both of the samples tested. However, the erosion properties do not correlate with moisture content across the two samples (as presented later).

Table 2 summarises for every erosion test at different depths: (i) the water content (by mass); (ii) the threshold velocity at 20 mm above the

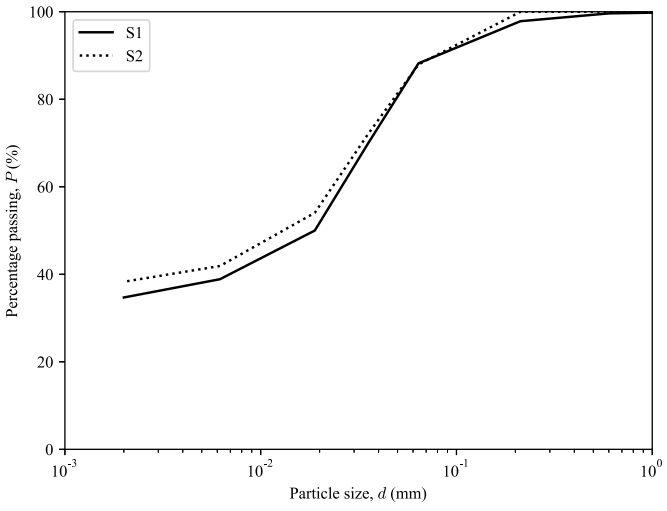

Fig. 4. Particle size distribution for sample S1 and S2.

Table 1
Properties of sediments tested.

Sample	z (m)	G_s (-)	d_{50} (mm)	Fines[+] (%)	Clay[x] (%)
S1	0 – 0.4	2.67	0.019	88	34
S2	0 – 0.4	2.63	0.013	88	38

[+] < 64 μm
[x] < 2 μm

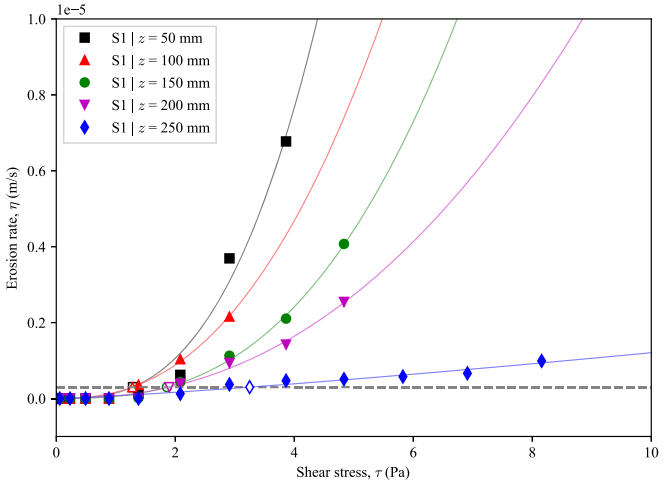

(a)

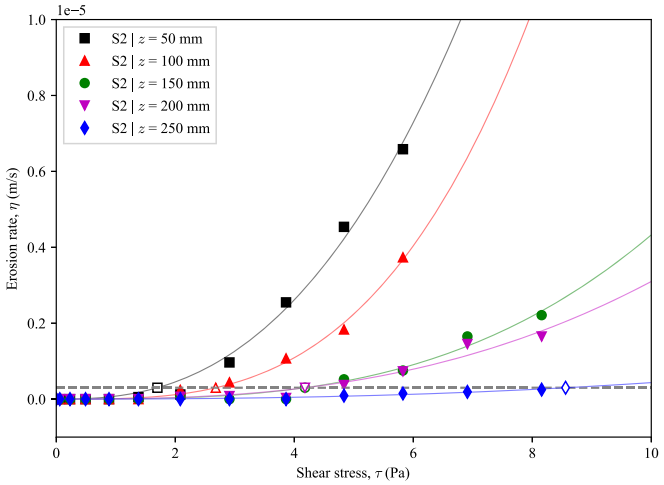

(b)

Fig. 5. Summary of erosion data for S1 and S2.

bed; (iii) the associated threshold shear stress; (iv) the threshold Shields parameter; and (v) the erosion rate fitting parameters M and n for Equation (4). During testing, erosion patterns across the samples were often intricately non-uniform, necessitating the need for averaging of measurements across the sample surface. Visual observations of the erosion onset agree reasonably well with the threshold shear stresses determined from the acoustic sensor measurements. In general, close to the threshold shear stress, the water became cloudy and very small particles were seen to move from the sample surface. As the shear stress increased well above threshold, small clumps being removed from the samples increased in size but remained in size below 1 mm.

At the highest shear stress tested, larger clumps were seen to be removed from the sample surface. These large clumps were removed sporadically and led to the loss of a significant volume of the sample. In other words, the erosion process resembled 'mass erosion' at this stage; as for example described in Winterwerp and Van Kesteren (2004). Zones with increased water content relative to the surrounding material had a tendency to erode sediment in a very short amount of time by mass erosion once the threshold was reached. In these zones of the sample, it appeared that once a particular spot was weakened (for example in the form of an eroding hole), mass erosion started from this spot and propagated along the sample in the 'streamwise' direction. Given the origin of the samples tested, it is possible that these clumps could come from the periphery of burrows (e.g. Kuo and Bolton (2013)).

Table 2
Erosion parameters including threshold velocity at 20 mm above bed and threshold shear stress.

Sample	z (m)	w (%)	U_{cr} (m/s)[x]	τ_{cr} (Pa)[+]	θ_{cr} (-)[+]	M (ms^{-1}Pa^{-n})	n (-)
S1	0.05	82.57	0.79	1.29	4.15	1.47e-07	2.85
	0.1	83.80	0.78	1.28	4.12	1.66e-07	2.41
	0.15	81.65	0.96	1.86	5.99	5.52e-08	2.73
	0.2	74.71	0.97	1.90	6.12	6.98e-08	2.28
	0.25	72.35	1.31	3.25	10.46	6.94e-08	1.24
S2	0.05	113.35	0.92	1.70	8.19	7.86e-08	2.53
	0.1	120.16	1.18	2.68	12.92	1.24e-08	3.23
	0.15	115.76	1.51	4.18	20.14	3.79e-09	3.06
	0.2	114.11	1.51	4.18	20.14	6.49e-09	2.68
	0.25	112.9	2.23	8.56	41.25	1.74e-09	2.40

[+] At η_{cr} ~3e-7 m/s
[x] 20 mm above bed

Fig. 6 compares the threshold conditions estimated using an empirical formula (known as the 'Shields curve') in dimensionless and dimensional form. The 'Shields curve' is often assumed to be a good predictor of threshold shear stress for non-cohesive sandy sediments with uniform particle distributions and rounded particles (Soulsby and Whitehouse, 1997). It is evident that for all subsamples the threshold shear stress is higher - by an order of magnitude - than that predicted by the 'Shields curve'. The erosion resistance of the material tested is therefore far larger (with 1.28 Pa for the smallest threshold shear stress) than would be predicted assuming a non-cohesive sediment with equivalent median particle size, as would be produced by a prediction using the 'Shields curve', for example.

The fact that the erosion testing results indicate that the samples tested have higher threshold shear stress than predicted by the 'Shields curve' is in broad agreement with previous measurements obtained from similar sediments (Mohr, 2015). In all of these types of test, surface erosion driven by particle-by-particle movement is difficult to observe with the naked eye due to the small grain sizes, however, mass erosion was certainly observed at higher shear stresses. Threshold shear stresses determined using measured erosion rates based on acoustic distance measurements showed good agreement with visual estimates of threshold shear stress. As shown in Fig. 7 and Fig. 8, the critical shear stress increases with increasing depth or reducing water content. There is however no consistent link between moisture content and erosion properties across the two samples. This observation is in agreement with erosion measurements reported by Mohr (2015), who also show that the functional relationship between threshold shear stress and water content is generally different for different sediments at the same moisture content.

It is clear from Fig. 6 to Fig. 8 - which compare samples from a single project location - that erosion properties of these type of natural sediment cannot be reliably estimated solely from geotechnical proxy parameters such as particle size or water content. According to Mohr et al. (2020) and Mohr et al. (2018), the most reliable link to a geotechnical property is with permeability, and hypothesise that this is due to the formation of the seepage forces beneath the eroding particles in fine-grained soils. However, it is not recommended to perform laboratory tests to determine permeability as a route to design erosion

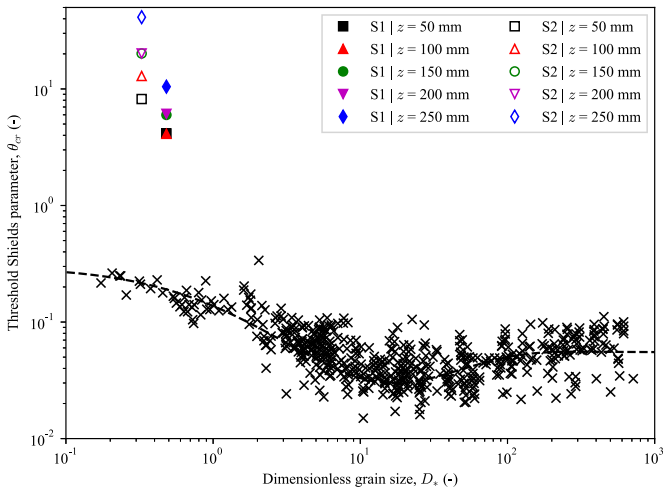

(a)

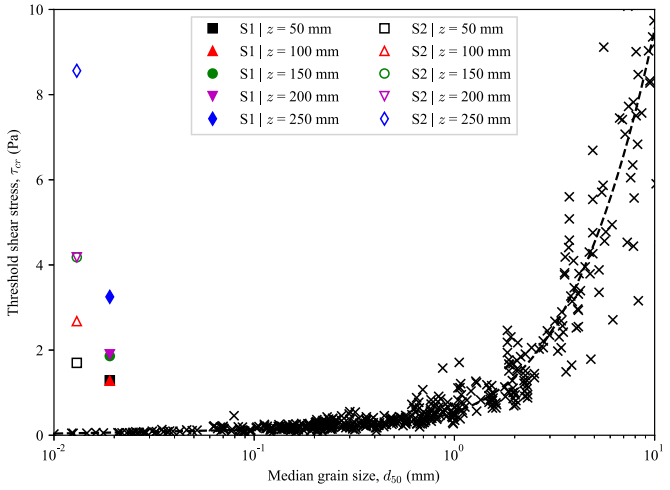

(b)

Fig. 6. Comparison of S1 and S2 with Shields curve (a) dimensionless and (b) dimensional.

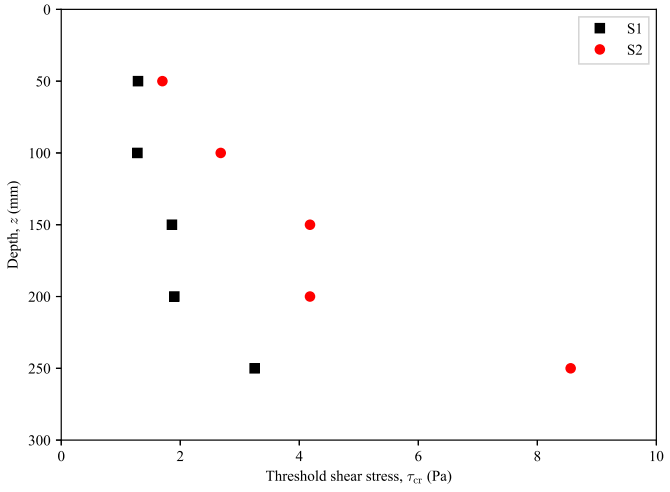

Fig. 7. Variation with depth of threshold shear stress for S1 and S2.

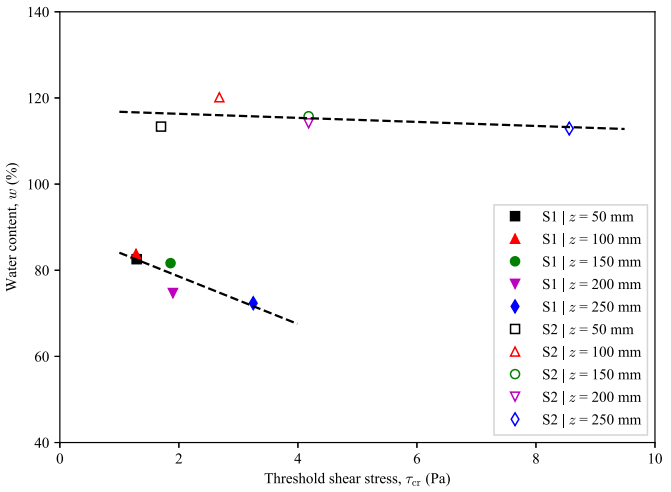

Fig. 8. Effect of water content on threshold shear stress for S1 and S2.

properties. It is more efficient to use an erosion flume to provide a direct and well-defined basis for selecting design values of erosion properties, as illustrated in this paper.

The deviation of the measured threshold shear stress from the 'Shields curve' is in agreement with previous measurements obtained from similar sediments (Mohr, 2015). Deviations from the 'Shields curve' generally occur for finer sediments, for which erosion testing is a more necessary requirement when characterising sediment mobility for design.

5. Discussion

The changes of the threshold shear stress and erosion rate with depth have significant implications for the scour assessment of subsea structure. These trends with depth affect, in particular: (i) the onset of scour; (ii) the scour hole depth; and (iii) the rate of scour, as discussed below:

- Conventional erosion tests indicate the average erosion characteristics over a sample depth of 200–250 mm (depending on sample length). This is because the sample tube is typically split length-ways and tested in an orientation rotated 90° from the in-situ condition in order to maximise the exposed sample surface area (e.g. Draper et al. (2017)). This may lead to higher threshold and lower erosion rate values compared to measurements from the top layer, if the erosion resistance increases with depth as observed here. The top layer in both samples appeared to be more susceptible to erosion than would be indicated by a single test, performed horizontally in the style adopted in typical erosion tests, where the erosion properties are effectively depth-averaged. For example, the averaged threshold shear stress over a depth from 50 mm to 250 mm (i.e. 200 mm length) for S1 and S2 is 1.92 Pa and 4.26 Pa, respectively. This erosion threshold when averaged over depth are greater compared with the uppermost layer for S1 and S2 by factors of 1.5 and 2.5 respectively.
- The results obtained from the portable erosion flume tests also show that with increasing depth the erosion threshold increases and this, therefore, may affect the progression of a developing scour hole. As a scour hole propagates with depth, it may encounter layers with higher erosion resistance which will limit the development of the scour hole. This is consistent with the observations of Mohr et al. (2016), where it was shown that scour hole depth decreases in finer sediments.
- Pipeline scour experiments performed on sediments from Australia's North West Shelf (NWS) have shown that the scour time scales are proportional to the measured erosion rates (Mohr et al., 2016). In

scenarios where the erosion rate decreases with depth, the scour hole development rate will reduce with the progression of the scour hole depth. The development of the scour hole may even be halted if the deepening of the hole reduces the applied shear stress to below the threshold shear stress.

To illustrate the implications of the issues outlined above, we developed a predictive methodology for scour beneath a subsea pipeline using erosion data from fine-grained sediments, following Mohr et al. (2016), additionally taking into account depth-related variation in erodibility. However, we note that depth-dependant erosion data can also be applied to scour assessments for any seabed structure in cohesive sediments (such as bridge piers as demonstrated in Briaud et al. (1999)) or even to predict coastal erosion processes (see Elsayed and Goseberg (2020) and Elsayed et al. (2021)).

Following Mohr et al. (2016), we take a 0.5 m (outside) diameter flowline and consider the implications on the scour hole development predictions of assuming a constant (depth-averaged) and depth-varying erosion rate for the S1 and S2 samples. Assuming that the flowline is subjected to a steady current of 0.8 m/s (referenced at 1 m above the seabed), and rests on a silty seabed (d_{50} = 0.02 mm, comparable to S1 and S2) we calculate a free-field shear stress of 0.67 Pa. The equilibrium scour depth is taken as 60% of the flowline diameter (which is consistent with a large range of experimental results in different sediments (e.g. Sumer et al. (2002), Kjeldsen et al. (1973)); and the shear stress under the pipeline is amplified by a factor of 6 (following Fredsøe and Hansen (1987)). The calculations to predict the evolution of a scour pit beneath the pipeline are given in Table 3 and proceed as follows:

- Calculate the equilibrium scour depth (S_e) for example based on the expression by Sumer et al. (2002), i.e. S/D = 0.6.
- Assess the amplified shear stress (τ_{amp}) so as to compute the erosion rate beneath the pipe (η_{avg} and η).
- Calculate the timescales for the fine grained sediment following Mohr et al. (2016). To calculate the timescales, two approaches are chosen: (i) averaged erosion rate over 250 mm depth (see η_{avg} in Table 3) and (ii) changing erosion rate with depth representative for the portable flume data (see η in Table 3). Calculation of the two time scales for averaged over depth and changing with depth, defined by the parameter T_{avg} and T, respectively, leads to the results in Table 3.
- The timescale parameter T represents the time for the scour hole to develop to 63% of the final value, following an exponential trend with time (Mohr et al., 2016).
- The progression of erosion depth with time can then be plotted using relations given in Mohr et al. (2016) and compared for the various scenarios, as shown in Fig. 9 for samples S1 and S2.

This calculation shows that the scour development considering different eroding layers is more rapid at shallow depth than the depth-averaged approach, which assumes a higher onset threshold shear stress and lower erosion rate for the surficial material. For the layered approach, as the scour hole progresses, the erosion rate for the presently exposed material is used. This means that as the depth increases the scour development slows down (by more than simply the general exponential decay of scour evolution in uniform material). Eventually, the erosion rate assumed in the depth-averaged approach becomes larger than that measured in the layered testing approach, which would

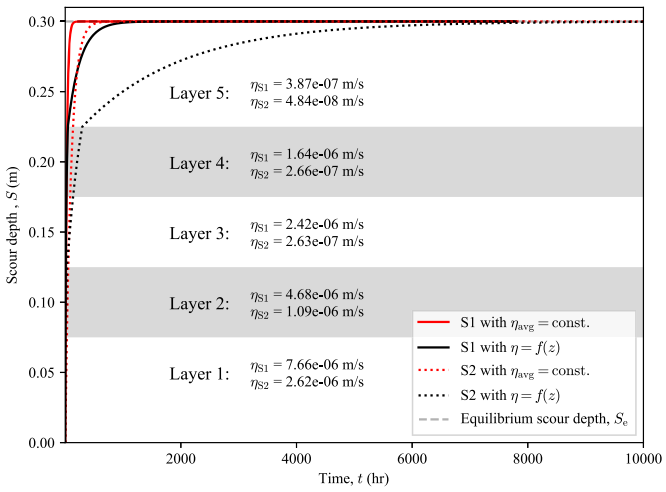

(a)

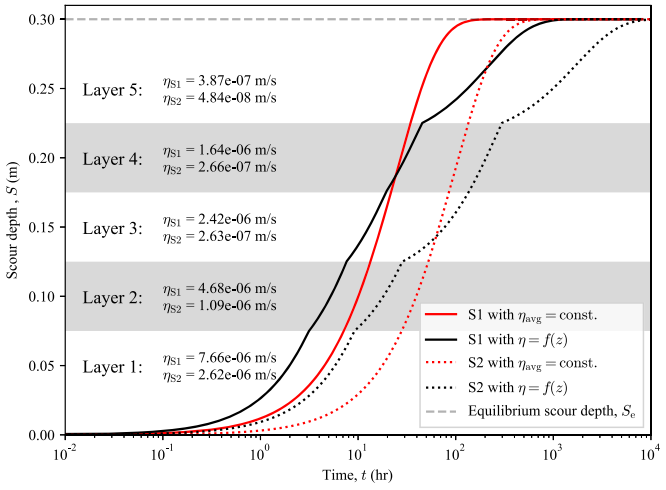

(b)

Fig. 9. Pipeline scour predictions using constant or depth varying erosion rates for sample S1 and S2.

Table 3
Pipeline scour parameters using constant or depth varying erosion rates for sample S1 and S2.

ID	No.	Depth	τ_{free} & τ_{amp}(Pa)	S_e(m)	η_{avg}(m/s)*	T_{avg}(s)*	η(m/s)+	T(s)+
	1	0 – 0.075					7.66e-06	3.92e+04
	2	0.075 – 0.125					4.68e-06	6.40e+04
S1	3	0.125 – 0.175	0.67&4.02	0.3	3.36e-06	8.94e+04	2.42e-06	1.24e+05
	4	0.175 – 0.225					1.64e-06	1.83e+05
	5	0.225 – 0.3					3.87e-07	7.74e+05
	1	0 – 0.075					2.62e-06	1.15e+05
	2	0.075 – 0.125					1.09e-06	2.75e+05
S2	3	0.125 – 0.175	0.67&4.02	0.3	8.57e-07	3.50e+05	2.63e-07	1.14e+06
	4	0.175 – 0.225					2.66e-07	1.13e+06
	5	0.225 – 0.3					4.84e-08	6.20e+06

* Averaged over depth
+ Changing with depth

lead to predictions of more rapid and extensive scour hole development than would be observed in reality. The implication of this is that in some instances there is the potential that scour remediation measures might be excessive if depth-averaged measurements alone are relied upon in design. This could have significant cost implications.

For example, if the layered testing approach were to be adopted, the time needed to reach equilibrium would increase from ~200 hr to ~1200 hr and ~700 hr to ~8000 hr for S1 and S2, respectively. This would be particularly important for larger subsea structures where scour hole development would be deeper than measured in these tests, because the influence of changing erosion resistance with depth would be even more important in those scenarios. Eventually, the increase in erosion resistance may even halt the deepening of the scour hole, yet this would not be captured by a single depth-averaged erosion measurement.

6. Conclusion

Seabed scour can significantly affect the performance and stability of subsea infrastructure in locations with potential sediment mobility. Utilising better predictive tools can mitigate the risk and lead to less cost-intensive measures for scour protection.

This paper introduces a newly-developed portable laboratory erosion flume that measures the erosion properties of tube samples in their natural orientation. This allows a depth resolution of the erosion properties so that a depth-dependant assessment of scour around subsea structure can be made.

The bulk properties were shown to systematically vary by a significant amount resulting in a increase in threshold shear stress and and a decrease in the rate of erosion which is in line with previous studies (see for more details Whitehouse et al. (2000). The erosion measurements presented in this report show that the erosion properties vary significantly over the uppermost ~300 mm of the seabed, to a degree that would significantly affect rates of scour propagation. For one sample the critical erosion onset velocity doubled over a 200 mm increase in depth, with the erosion rate falling by an order of magnitude. This is a detail that is not captured by other devices that test a tube sample in a horizontal orientation rather than the natural vertical orientation. Horizontal split samples provide results that effectively average the erosion properties with depth into a single measurement, and such results could lead to erroneous predictions of scour rate. For example, a thin layer with higher erosion resistance could prevent further deepening of a scour feature. However, in conventional split sample erosion tests only the average erosion properties are measured, so effects such as this 'armouring' from a thin layer cannot be detected and used beneficially in design. This high resolution with depth is an aspect that can only be explored using the new portable erosion flume. Finally, we recommend that further research in the form of scour model testing in fine-grained sediments should be undertaken in order to validate our modified scour predictions following the methodology suggested by Briaud et al. (1999) and Mohr et al. (2016).

CRediT authorship contribution statement

Henning Mohr: Conceptualization, Data curation, Formal analysis, Writing - original draft. **Samuel A. Stanier:** Formal analysis, Writing - original draft. **David J. White:** Writing - review & editing. **Matthew Kuo:** Writing - review & editing.

Declaration of Competing Interest

The authors declare that they have no known competing financial interests or personal relationships that could have appeared to influence the work reported in this paper.

Acknowledgments

This research was conducted by the Wave Energy Research Centre and jointly funded by The University of Western Australia and the Western Australian Government, via the Department of Primary Industries and Regional Development (DPIRD). The work was also partly supported by the UK's EPSRC Offshore Renewable Energy Supergen Hub (grant EP/S000747/1).

Supplementary material

Supplementary material associated with this article can be found, in the online version, at 10.1016/j.apor.2021.102721

References

Amos, C.L., Grant, J., Daborn, G., Black, K., 1992. Sea carousel benthic, annular flume. Estuar. Coast. Shelf. Sci. 34 (6), 557–577.
Briaud, J.-L., Ting, F.C., Chen, H., Gudavalli, R., Perugu, S., Wei, G., 1999. Sricos: prediction of scour rate in cohesive soils at bridge piers. J. Geotech. Geoenviron. Eng. 125 (4), 237–246.
Buffington, J.M., Montgomery, D.R., 1997. A systematic analysis of eight decades of incipient motion studies, with special reference to gravel-bedded rivers. Water Resour. Res. 33 (8), 1993–2029.
Colebrook, C.F., White, C.M., 1937. Experiments with fluid friction in roughened pipes. Proceedings of the Royal Society of London 161 (906), 367–381.
Debnath, K., Nikora, V., Aberle, J., Westrich, B., Muste, M., 2007. Erosion of cohesive sediments: resuspension, bed load, and erosion patterns from field experiments. J. Hydraul. Eng. 133 (5), 508–520.
Draper, S., Harris, J.M., Cheng, L., White, D.J., 2017. Seabed processes: sediment transport, scour, and sedimentation. Encyclopedia of Maritime and Offshore Engineering 1–11.
Elsayed, S.M., Goseberg, N., 2020. Role of spatial variability of soil resistance in alongshore variability of coastal barriers response to superstorm surges. Coastal Engineering Proceedings (36v), 41.
Elsayed, S.M., Oumeraci, H., Goseberg, N., 2021. Integrating spatial variability of soil properties in xbeach to predict erosion and breaching of natural coastal barriers under storm surges. Under preparation.
Fredsøe, J., Hansen, E.A., 1987. Lift forces on pipelines in steady flow. Journal of Waterway, Port, Coastal, and Ocean Engineering 113 (2), 139–155.
Fredsøe, J., Sumer, B.M., Arnskov, M.M., 1992. Time scale for wave/current scour below pipelines. Int. J. Offshore Polar Eng. 2 (1), 13–17.
Gust, G., Morris, M.J., 1989. Erosion thresholds and entrainment rates of undisturbed in situ sediments. Journal of Coastal Research 87–99.
Jacobs, W., Le Hir, P., Van Kesteren, W., Cann, P., 2011. Erosion threshold of sand–mud mixtures. Cont. Shelf Res. 31 (10), S14–S25.
Jepsen, R., Roberts, J., Lick, W., 1997. Effects of bulk density on sediment erosion rates. Water Air Soil Pollut. 99 (1–4), 21–31.
Kern, U., Haag, I., Schürlein, V., Holzwarth, M., Westrich, B., 1999. Ein Strömungskanal zur Ermittlung der tiefenabhängigen Erosionsstabilität von Gewässersedimenten: Das SETEG-system. Wasserwirtschaft 89 (2), 72–77.
Kjeldsen, S., Gjorsvik, O., Bringaker, K., Jacobsen, J., 1973. Local scour near offshore pipelines. Proceedings of the Second International Conference on Port and Ocean Engineering Under Arctic Conditions.
Kuo, M., Bolton, M., 2013. The nature and origin of deep ocean clay crust from the gulf of guinea. Géotechnique 63 (6), 500–509.
Leckie, S.H., Draper, S., White, D.J., Cheng, L., Fogliani, A., 2015. Lifelong embedment and spanning of a pipeline on a mobile seabed. Coastal Eng. 95, 130–146.
Lee, C.W., Chen, J.H., 2007. The characteristics of rim-driven propulsor's flow field. Proc. 5th International Symposium on Turbulence and Shear Flow Phenomena, Vol. 2, pp. 607–611.
Maa, J.-Y., Wright, L., Lee, C.-H., Shannon, T., 1993. VIMS sea carousel: a field instrument for studying sediment transport. Mar. Geol. 115 (3–4), 271–287.
Mao, Y., 1986. The interaction between a pipeline and an erodible bed.. Technical University of Denmark, Denmark. Ph.D. thesis.
McNeil, J., Taylor, C., Lick, W., 1996. Measurements of erosion of undisturbed bottom sediments with depth. J. Hydraul. Eng. 122 (6), 316–324.
Mitchener, H., Torfs, H., 1996. Erosion of mud/sand mixtures. Coastal Eng. 29 (1–2), 1–25.
Mohr, H., 2015. Erosion and scour behaviour of marine sediments. University of Western Australia, Australia. Ph.D. thesis.
Mohr, H., Draper, S., White, D.J., Cheng, L., 2016. Predicting the rate of scour beneath subsea pipelines in marine sediments under steady flow conditions. Coastal Eng. 110, 111–126.
Mohr, H., Draper, S., White, D.J., Cheng, L., 2018. The influence of permeability on the erosion rate of fine-grained marine sediments. Coastal Eng. 140, 124–135.
Mohr, H., Draper, S., White, D.J., Cheng, L., 2020. The effect of permeability on the erosion threshold of fine-grained sediments. Coastal Eng. 163, 103813.
Noack, M., Gerbersdorf, S.U., Hillebrand, G., Wieprecht, S., 2015. Combining field and laboratory measurements to determine the erosion risk of cohesive sediments best. Water (Basel) 7 (9), 5061–5077.

Nowell, A.R., Hollister, C.D., 1985. The objectives and reationale of hebble. Mar. Geol. 66 (1–4), 1–11.
Pandey, M., Sharma, P., Ahmad, Z., Singh, U.K., 2017. Evaluation of existing equations for temporal scour depth around circular bridge piers. Environ. Fluid Mech. 17 (5), 981–995.
Rambabu, M., Rao, S.N., Sundar, V., 2003. Current-induced scour around a vertical pile in cohesive soil. Ocean Eng. 30 (7), 893–920.
Ravens, T.M., Gschwend, P.M., 1999. Flume measurements of sediment erodibility in boston harbor. J. Hydraul. Eng. 125 (10), 998–1005.
Roberts, J.D., Jepsen, R., Gotthard, D., Lick, W., 1998. Effects of particle size and bulk density on erosion of quartz particles. J. Hydraul. Eng. 124 (12), 1261–1267.
Roberts, J.D., Jepsen, R.A., James, S.C., 2003. Measurements of sediment erosion and transport with the adjustable shear stress erosion and transport flume. J. Hydraul. Eng. 129 (11), 862–871.
Sleath, J.F., 1984. Sea bed mechanics. John Wiley and Sons Inc., New York, NY.
Soulsby, R.L., Whitehouse, R.J.S., 1997. Threshold of sediment motion in coastal environments. Proc. 13th Australasian Coastal and Ocean Engineering Conference and 6th Australasian Port and Harbour Conference 1, 145.
Sumer, B.M., et al., 2002. The mechanics of scour in the marine environment. World Scientific.
Tom, J., Draper, S., White, D., O'Neill, M., et al., 2016. Risk-based assessment of scour around subsea infrastructure. Offshore Technology Conference.
Whitehouse, R., 1998. Scour at marine structures: A manual for practical applications. Thomas Telford.
Whitehouse, R., Soulsby, R., Roberts, W., Mitchener, H., 2000. Dynamics of estuarine muds. Thomas Telford.
Winterwerp, J.C., Van Kesteren, W.G., 2004. Introduction to the physics of cohesive sediment dynamics in the marine environment. Elsevier.
Yakovlev, A.Y., Sokolov, M.A., Marinich, N.V., 2011. Numerical design and experimental verification of a rim-driven thruster. Proc. 2nd International Symposium on Marine Propulsors, pp. 1–7.
Ye, Z., Cheng, L., Zang, Z., 2011. Experimental study of erosion threshold of reconstituted sediments. Proc. 30th International Conference on Offshore Mechanics and Arctic Engineering 44397, 973–983.
Young, R.A., 1977. Seaflume: a device for in-situ studies of threshold erosion velocity and erosional behavior of undisturbed marine muds. Mar. Geol. 23 (1–2), M11–M18.